Coexisting rogue waves within the (2+1)-component long-wave–short-wave resonance

Shihua Chen,[1] Jose M. Soto-Crespo,[2] and Philippe Grelu[3]
[1]*Department of Physics, Southeast University, Nanjing 211189, China*
[2]*Instituto de Óptica, Consejo Superior de Investigaciones Científicas (CSIC), Serrano 121, Madrid 28006, Spain*
[3]*Laboratoire Interdisciplinaire Carnot de Bourgogne, U.M.R. 6303 C.N.R.S., Université de Bourgogne, 9 avenue A. Savary, Boîte Postale 47870, Dijon Cedex 21078, France*
(Received 9 May 2014; published 15 September 2014)

The coexistence of two different types of fundamental rogue waves is unveiled, based on the coupled equations describing the (2+1)-component long-wave–short-wave resonance. For a wide range of asymptotic background fields, each family of three rogue wave components can be triggered by using a slight deterministic alteration to the otherwise identical background field. The ability to trigger markedly different rogue wave profiles from similar initial conditions is confirmed by numerical simulations. This remarkable feature, which is absent in the scalar nonlinear Schrödinger equation, is attributed to the specific three-wave interaction process and may be universal for a variety of multicomponent wave dynamics spanning from oceanography to nonlinear optics.

DOI: 10.1103/PhysRevE.90.033203 PACS number(s): 05.45.Yv, 47.20.Ky, 47.35.−i, 47.54.−r

Rogue waves, a term originally coined to provide a vivid description of the mysterious monstrous ocean waves [1], have recently attracted much interest in the study of their fundamental origin and complex dynamics [2,3]. In addition to being manifested in the open ocean and deep water related experiments [4,5], these extreme wave events were also observed in a wide class of physical systems, including capillary waves and surface ripples [6,7], plasmas [8], optical fibers [9,10], mode-locked lasers [11], and filaments [12]. These studies have uncovered general features of nonlinearity and complexity shared by rogue waves, e.g., they are extremely large and steep compared with typical events, occur in a nonlinear medium, and follow an unusual L-shaped statistics [9,11–13]. Despite these diverse features, mathematical solutions of rogue waves can be expressed as rational functions localized in both space and time. One typical example is the Peregrine soliton [14], a well-known rogue wave prototype in various experimental fields [4,8,10], which is the lowest-order rational solution to the nonlinear Schrödinger (NLS) equation.

Following the need to model complex physical systems more precisely, it has become important to study rogue wave phenomena beyond the framework of the NLS equation. Recent developments have taken into account dissipative effects [11,15,16], included higher-order nonlinear terms [17–19], or considered the coupling between several fields [20–25]. The latter investigations have led to the discovery of intricate rogue wave structures that are generally unattainable in the scalar models. In particular, we showed in Ref. [25] that the long-wave–short-wave (LWSW) resonance interaction can result in stable dark and bright rogue waves in spite of the onset of modulational instability (MI). This finding brings about the possibility to observe dark rogue waves in LWSW resonance systems such as negative index media [26] and capillary-gravity waves [6,27].

Basically, the LWSW resonance is a general parametric process that manifests when the group velocity of the short wave matches the phase velocity of the long wave [28]. It has been predicted in different disciplines such as fluid dynamics [27], plasma physics [29], oceanography [30], and nonlinear optics [26,31]. Early works showed that both the LWSW and the NLS equations could be obtained from the same Davey-Stewartson system under the appropriate parameter conditions [27,32,33], although the former is currently less popular in use than the latter.

In fact, it is possible to consider multiple interactions in a vector LWSW resonance system, corresponding to the interaction between N short waves and one long interfacial wave. We shall refer to such a vector system as the $(N+1)$-component LWSW resonance system [34–36]. With $N = 2$, the intrinsic complexity of the LWSW resonance system leads to the discovery of original vector multisoliton dynamics [37]. We anticipated that, if rogue wave solutions could be found in the (2+1)-component (C) LWSW resonance model, they would feature unique properties.

In this paper, we report the *compossibility* of two different families of fundamental (first-order) rogue wave solutions, which exist simultaneously in the (2+1)-C LWSW resonance system. We demonstrate explicitly that, due to the specific three-wave resonance, one family of three rogue wave components can coexist with the other for the same initial parameters. Finally, the robustness of these coexisting rogue waves as well as the ability to trigger them is confirmed numerically.

The nonlinear interaction between two complex short-wave field envelopes, u and v, and the real long-wave field, ϕ, can be modeled by the (2+1)-C LWSW resonance equation, expressed in a normalized form

$$\begin{aligned} iu_t + \tfrac{1}{2}u_{xx} + u\phi &= 0, \\ iv_t + \tfrac{1}{2}v_{xx} + v\phi &= 0, \\ \phi_t - (|u|^2 + |v|^2)_x &= 0, \end{aligned} \tag{1}$$

where t and x are two independent evolution variables and the subscripts stand for the partial derivatives. Here, the first two of Eq. (1) have been arranged into a form similar to the standard NLS equation, making it clear that the nonlinearity experienced by each short wave is driven by the long-wave field, ϕ, rather than by $|u|^2$ or $|v|^2$. In optical contexts, while the short-wave components u and v are called optical waves, the long-wave component ϕ could be thought of as the induced optical rectification [31] or the low-frequency

terahertz wave [26]. As one can check, this system of equations can be readily cast into a 4×4 linear eigenvalue problem (one can refer to the Lax pair provided in Ref. [38] or refer to Ref. [39] for technical details) and thus can be solved, although cumbersome, by use of the inverse scattering transform or Darboux transformation.

Here we exploited the Hirota bilinear method, which is expedient and efficient when the trial solutions can be easily deduced from the known solutions of a less complicated system [25]. After a little algebra, we obtain the exact fundamental rogue wave solutions of Eq. (1) as

$$u = u_0\left\{1 - \frac{2in^2t + 2i(m-k)(x-mt) + 1}{[n^2 + (m-k)^2]\left[(x-mt)^2 + n^2t^2 + \frac{1}{4n^2}\right]}\right\}, \tag{2}$$

$$v = v_0\left\{1 - \frac{2in^2t + 2i(m-K)(x-mt) + 1}{[n^2 + (m-K)^2]\left[(x-mt)^2 + n^2t^2 + \frac{1}{4n^2}\right]}\right\}, \tag{3}$$

$$\phi = b + 2\frac{n^2t^2 - (x-mt)^2 + \frac{1}{4n^2}}{\left[(x-mt)^2 + n^2t^2 + \frac{1}{4n^2}\right]^2}, \tag{4}$$

where the initial plane waves u_0, v_0 are defined by their respective amplitude (a, A), wave number (k, K), and frequency (ω, Ω) according to

$$u_0(t,x) = a\exp(ikx - i\omega t), \tag{5}$$

$$v_0(t,x) = A\exp(iKx - i\Omega t). \tag{6}$$

The dispersion relations for the above seeding plane waves are given by $\omega = \frac{1}{2}k^2 - b$ and $\Omega = \frac{1}{2}K^2 - b$ (here $b \geqslant 0$ defines the background of the real long-wave field). The real parameters m and n in Eqs. (2)–(4) must satisfy

$$m + \frac{a^2[n^2 - (m-k)^2]}{[n^2 + (m-k)^2]^2} + \frac{A^2[n^2 - (m-K)^2]}{[n^2 + (m-K)^2]^2} = 0, \tag{7}$$

$$\frac{1}{2} + \frac{a^2(m-k)}{[n^2 + (m-k)^2]^2} + \frac{A^2(m-K)}{[n^2 + (m-K)^2]^2} = 0. \tag{8}$$

As a result, for given initial plane-wave parameters, one can use Eqs. (7) and (8) to determine the values of m and n, hence to determine the rogue wave solutions (2)–(4). Since the above solutions involve n^2 only, thus for clarity we shall assume $n > 0$ below.

Equations (2)–(4) represent general families of fundamental rogue wave solutions of Eq. (1), with intricate rogue wave structures that resemble those displayed in the two-wave resonance case [25]. Indeed, when one field vanishes, these solutions can be readily reduced to those presented in Ref. [25]. In most cases, m and n are implicitly determined by the system of coupled algebraic equations (7) and (8), and thus one needs to solve for them numerically in order to find all possible rogue wave states.

Let us first explore the asymptotic behaviors of Eqs. (7) and (8) analytically as $K \to \pm\infty$, for a given k value without loss of generality. There are the following two considerations. On one hand, for a finite m in the limit of $K \to \pm\infty$, the third term on the left-hand side of both Eqs. (7) and (8) can be neglected, resulting in

$$2(m-k)(2m-k)^2 + a^2 = 0, \tag{9}$$

$$n = \sqrt{(m-k)(3m-k)}. \tag{10}$$

These give the asymptotic solutions, m and n, of Eqs. (7) and (8) provided that $k \leqslant 3(2a^2)^{1/3}/2 \approx 1.89a^{2/3}$. On the other hand, if n is kept finite but $m \sim K$ as $K \to -\infty$, we can also reduce Eqs. (7) and (8) into

$$2(m-K)(2m-K)^2 + A^2 = 0, \tag{11}$$

$$n = \sqrt{(m-K)(3m-K)}. \tag{12}$$

In this case, the asymptotic solutions, m and n, will be independent of k for K approaching $-\infty$. It is of interest to note that the above two sorts of asymptotic behaviors are able to exist simultaneously if $k \leqslant 3(2a^2)^{1/3}/2$, otherwise only the second sort can survive.

We solved Eqs. (7) and (8) numerically for all allowed (m,n), using $k = 0$, -1, or 2, and letting $A = a = 1$ for simplicity. These results are plotted in Figs. 1(a) and 1(b),

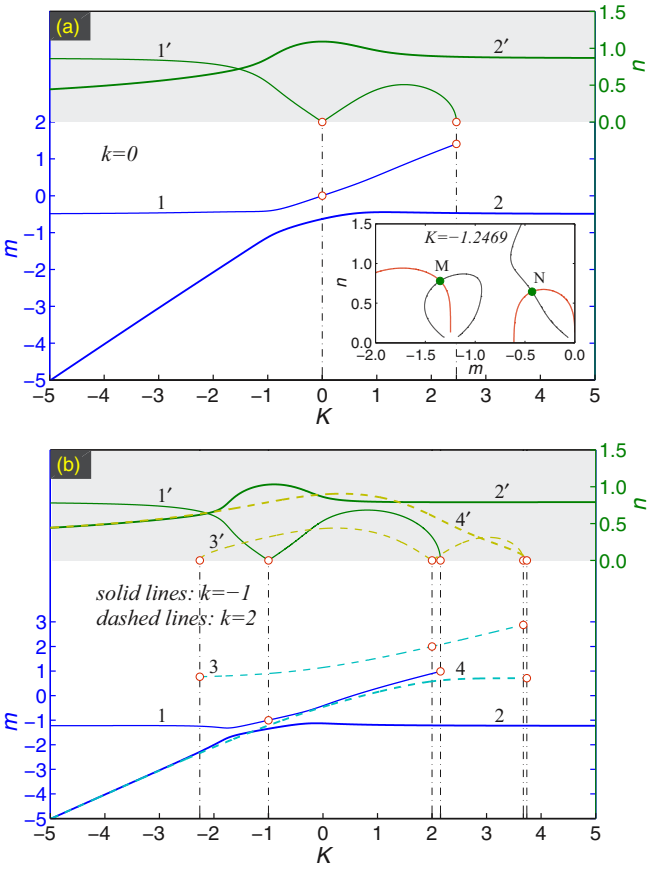

FIG. 1. (Color online) Allowed real parameters m and n versus K for (a) $k = 0$ and (b) $k = -1$ (solid lines) or $k = 2$ (dashed lines). The inset in (a) shows the existence of two pairs of real solutions (m,n) of Eqs. (7) and (8) for $K = -1.2469$.

showing that as $k = 0$ or -1, m and n have valid values in the whole regime of K, with the asymptotic behaviors exactly described by Eqs. (9)–(12) [see the solid lines $(1,1')$ and $(2,2')$ therein]. However, once k is larger than 1.89 (here we chose $k = 2$), the valid domain of K will be greatly reduced and only the asymptotic behavior given by Eqs. (11) and (12) remains, as indicated by the dashed lines $(3,3')$ and $(4,4')$ in Fig. 1(b). We should point out that all the red circles in Figs. 1(a) and 1(b) must be excluded, because they give the trivial value $n = 0$ that is not allowed by the rogue wave solutions (2)–(4).

Intriguingly, Fig. 1 reveals that for given initial plane-wave parameters, coexisting rogue wave solutions are possible. Specifically, as seen in Fig. 1(a), when $k = 0$ and $K < 2.4600$ (truncated to four decimal places and the same below), each nonzero K value yields two sets of valid (m,n) which correspond to two coexisting rogue wave families. This can be understood from the inset in Fig. 1(a) where the n versus m trajectory of Eq. (7) (black line) can intersect that of Eq. (8) (red line) twice for $K = -1.2469$. In the same way, Fig. 1(b) shows that there exist two different families of rogue waves for $k = -1$ and $K < 2.1544$ (solid lines), or for $k = 2$ and $-2.2586 < K < 3.6734$ (dashed lines), of course excluding the decoupled case $K = k$. These remarkable coexisting behaviors can be reminiscent of the bistable states occurring in soliton evolutions [40–45], although typically rogue waves are transients while solitons are stationary states. As an illustration, we demonstrate in Fig. 2 the formation of the coexisting rogue wave states at the points M $(-1.3514, 0.7803)$ and N $(-0.4287, 0.6442)$ in the inset in Fig. 1(a). Here,

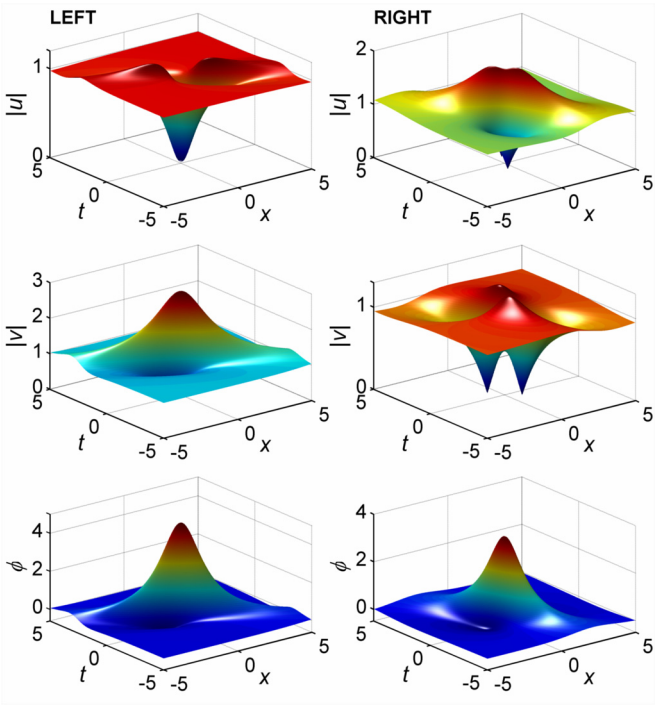

FIG. 2. (Color online) Two distinct yet fundamental rogue wave families for identical initial plane-wave parameters (letting $b = 0$). The left (right) column illustrates the rogue wave family developed at the M (N) point, as seen in the inset in Fig. 1(a).

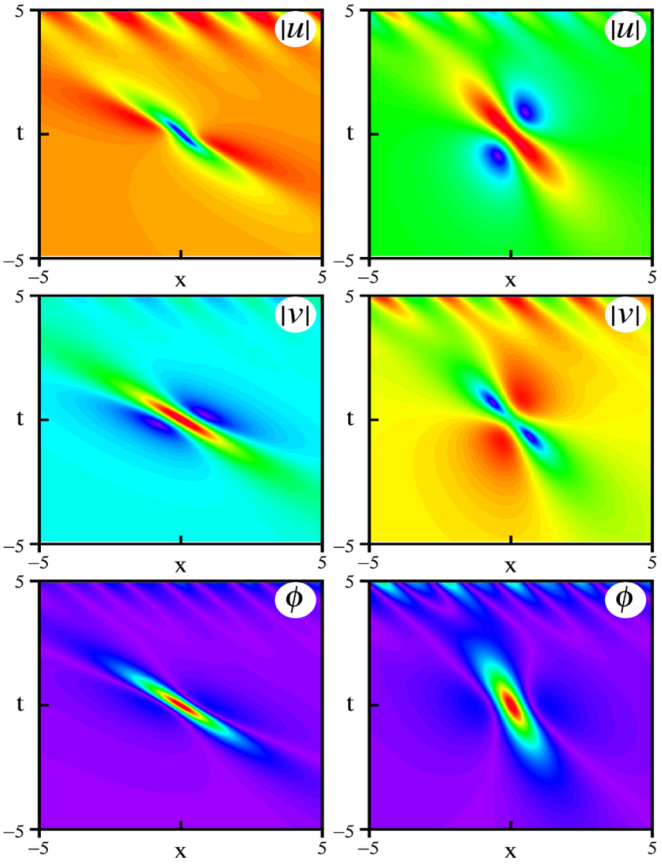

FIG. 3. (Color online) Numerical results showing the stability of two coexisting rogue wave families against initial white-noise perturbation, under otherwise identical conditions as in Fig. 2. The contour plots have the same layout as in Fig. 2.

the value of $K = -1.2469$ was chosen so that the $|u|$ field component may feature a black rogue wave structure, namely, can fall to zero in the dip center. It is shown that the rogue wave family at the M point (see left column) consists of black, bright, and bright structures for the corresponding three field components, while the one at the N point (see right column) takes a different combination of rogue wave structures. Obviously, these two families of fundamental rogue waves can coexist for the same initial parameters.

It is noteworthy that similar analytical solutions for the vector LWSW equations were recently given in Ref. [38], but those only correspond to the special case of our solutions, i.e., to Eqs. (2)–(4) with $K = b = 0$. In particular, the remarkable coexisting rogue wave behaviors that we are primarily concerned about were not shown there.

We have also performed extensive numerical simulations to study the formation, the stability, and the triggering characteristics of these coexisting rogue wave families. First, we solved the underlying model equation (1) by using a split-step Fourier method [25], with the analytical solutions (2)–(4) at $t = -5$ as initial conditions. These initial conditions correspond to faint perturbations of the asymptotic plane waves. We corroborated that our numerical code gave precisely the solution profiles predicted analytically until $t = 5$. Secondly, we studied numerically the stability of the rogue wave solutions by perturbing the above initial conditions. We multiplied the real and imaginary

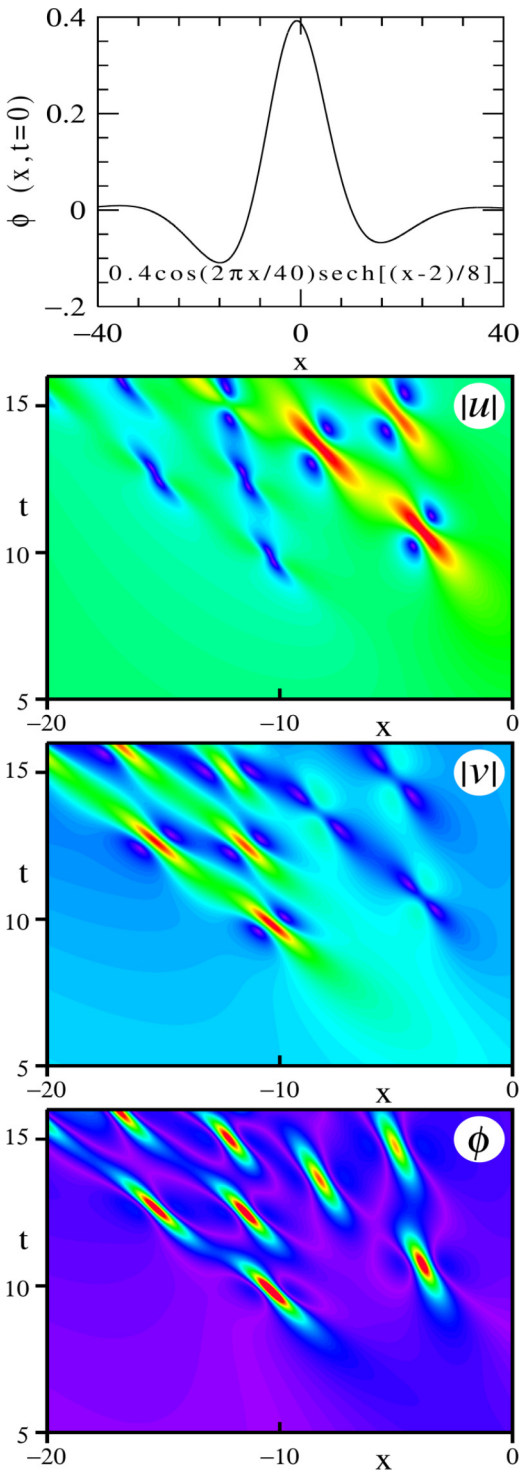

FIG. 4. (Color online) Excitation of two different families of fundamental rogue waves from a slight deterministic alteration to the otherwise identical background of the ϕ field. The top panel represents the initial profile of ϕ and the lower ones display the evolution of the three field components with time.

parts of both the u and v fields, and the real ϕ field by the factor $[1 + \mu r_i(x)]$ $(i = 1,2,\ldots,5)$, respectively, where $r_i(x)$ are uncorrelated random functions uniformly distributed in the interval $[-0.5,0.5]$, and μ is a constant defining the noise level (here we used $\mu = 10^{-4}$). Our simulation results are illustrated in Fig. 3, where for comparison we adopted the same initial parameters and the same layout as in Fig. 2. It is revealed that these two coexisting rogue wave families are stable on an unstable background, despite the fact that the MI tends to interfere strongly with the trailing edge of the localized solutions after some propagation time.

Thirdly, in order to see whether these rogue wave solutions would be easily triggered in realistic conditions, we intended to excite them numerically by using initial conditions significantly different from the exact solution profiles. To reduce the number of variables to play with, we used the plane-wave solutions (5) and (6) at $t = 0$ as initial conditions for u and v, each with the amplitude and wave number as used in Fig. 2 or 3, and the ansatz $\phi(t = 0,x) = p\cos(2\pi x/q)\mathrm{sech}[(x - x_0)/w]$, with p, q, x_0, and w being free parameters. Surprisingly, for certain of these free parameters, we found it possible to excite both types of fundamental rogue waves on a background. An example is provided with Fig. 4, where the initial condition $\phi(t = 0,x)$ is plotted in the top panel. In the evolution plots for $|u|$, $|v|$, and ϕ, the first five time units have been removed, as hardly no visible changes appear on the chosen scale. Then, at around $t = 10$, there appear simultaneously two markedly different rogue wave types, well separated and corresponding to those shown in Fig. 3. This demonstrates further, from the numerical perspective, the coexistence of diverse fundamental rogue waves. The temporal evolution that follows features additional rogue wave dynamics, all with a combination of both rogue wave types. The latter behavior could be linked to the existence of high-order multiple rogue wave solutions of Eq. (1), in analogy to the multiple rogue wave solutions found within the scalar NLS equation [46–48]. These subsequent multiple rogue waves could also be triggered by the onset of MI, which promotes quasiperiodic structures by patterning the continuous-wave background. Our other simulation results suggest that a deterministic change of the above asymmetric profile of ϕ could trigger either of the rogue wave types as well.

In conclusion, we have unveiled the remarkable feature that different fundamental rogue wave solutions of the (2+1)-C LWSW resonance system could coexist for the same initial plane-wave parameters. A slight change in the initial condition is able to make the rogue wave type hop from one family to the other. The stability of these coexisting rogue wave solutions was numerically proven to be strong enough that they can develop in the presence of noise. We attributed such a compossibility to the specific three-wave interaction process that occurs universally in many multicomponent systems. Finally, numerical simulations have indicated the tendency to generate multiple, or high-order, vector rogue wave events. The last point opens the door to further theoretical and numerical investigations.

This work was partially supported by the National Natural Science Foundation of China (Grants No. 11174050 and No. 11474051), the Natural Science Foundation of Jiangsu Province of China (Grant No. BK2011586), and the Agence Nationale de la Recherche, France (projects ANR-2010-BLANC-0417-01 and ANR-2012-BS04-0011). The work of J.M.S.C. was supported by MINECO (Spain) under Contracts No. FIS2009-09895 and No. TEC2012-37958-C02-02.

[1] C. Kharif, E. Pelinovsky, and A. Slunyaev, *Rogue Waves in the Ocean* (Springer, Berlin, 2009).

[2] M. Onorato, S. Residori, U. Bortolozzo, A. Montina, and F. T. Arecchi, Phys. Rep. **528**, 47 (2013).

[3] N. Akhmediev, J. M. Dudley, D. R. Solli, and S. K. Turitsyn, J. Opt. **15**, 060201 (2013).

[4] A. Chabchoub, N. P. Hoffmann, and N. Akhmediev, Phys. Rev. Lett. **106**, 204502 (2011).

[5] A. Chabchoub, N. Hoffmann, M. Onorato, and N. Akhmediev, Phys. Rev. X **2**, 011015 (2012).

[6] M. Shats, H. Punzmann, and H. Xia, Phys. Rev. Lett. **104**, 104503 (2010).

[7] H. Xia, T. Maimbourg, H. Punzmann, and M. Shats, Phys. Rev. Lett. **109**, 114502 (2012).

[8] H. Bailung, S. K. Sharma, and Y. Nakamura, Phys. Rev. Lett. **107**, 255005 (2011).

[9] D. R. Solli, C. Ropers, P. Koonath, and B. Jalali, Nature (London) **450**, 1054 (2007).

[10] B. Kibler, J. Fatome, C. Finot, G. Millot, F. Dias, G. Genty, N. Akhmediev, and J. M. Dudley, Nat. Phys. **6**, 790 (2010).

[11] C. Lecaplain, Ph. Grelu, J. M. Soto-Crespo, and N. Akhmediev, Phys. Rev. Lett. **108**, 233901 (2012).

[12] S. Birkholz, E. T. J. Nibbering, C. Brée, S. Skupin, A. Demircan, G. Genty, and G. Steinmeyer, Phys. Rev. Lett. **111**, 243903 (2013).

[13] N. Akhmediev, A. Ankiewicz, and M. Taki, Phys. Lett. A **373**, 675 (2009).

[14] D. H. Peregrine, J. Aust. Math. Soc., Ser. B, Appl. Math. **25**, 16 (1983).

[15] J. M. Soto-Crespo, Ph. Grelu, and N. Akhmediev, Phys. Rev. E **84**, 016604 (2011).

[16] Ph. Grelu and N. Akhmediev, Nat. Photonics **6**, 84 (2012).

[17] A. Ankiewicz, J. M. Soto-Crespo, and N. Akhmediev, Phys. Rev. E **81**, 046602 (2010).

[18] U. Bandelow and N. Akhmediev, Phys. Rev. E **86**, 026606 (2012).

[19] S. Chen, Phys. Rev. E **88**, 023202 (2013).

[20] Y. Ohta and J. Yang, Phys. Rev. E **86**, 036604 (2012).

[21] F. Baronio, A. Degasperis, M. Conforti, and S. Wabnitz, Phys. Rev. Lett. **109**, 044102 (2012).

[22] S. Chen and L.-Y. Song, Phys. Rev. E **87**, 032910 (2013).

[23] K. W. Chow, H. N. Chan, D. J. Kedziora, and R. H. J. Grimshaw, J. Phys. Soc. Jpn. **82**, 074001 (2013).

[24] F. Baronio, M. Conforti, A. Degasperis, and S. Lombardo, Phys. Rev. Lett. **111**, 114101 (2013).

[25] S. Chen, Ph. Grelu, and J. M. Soto-Crespo, Phys. Rev. E **89**, 011201(R) (2014).

[26] A. Chowdhury and J. A. Tataronis, Phys. Rev. Lett. **100**, 153905 (2008).

[27] V. D. Djordjevic and L. G. Redekopp, J. Fluid Mech. **79**, 703 (1977).

[28] D. J. Benney, Stud. Appl. Math. **56**, 81 (1977).

[29] V. E. Zakharov, Zh. Eksp. Teor. Fiz. **62**, 1745 (1972) [Sov. Phys. JETP **35**, 908 (1972)].

[30] M. S. Longuet-Higgins, J. Fluid Mech. **177**, 293 (1987).

[31] T. Colin and D. Lannes, Duke Math. J. **107**, 351 (2001).

[32] C. Babaoglu, Chaos Solitons Fractals **38**, 48 (2008).

[33] A. Davey and K. Stewartson, Proc. R. Soc. London, Ser. A **338**, 101 (1974).

[34] Y. Ohta, K. Maruno, and M. Oikawa, J. Phys. A: Math. Theor. **40**, 7659 (2007).

[35] H. Borluk and S. Erbay, IMA J. Appl. Math. **76**, 582 (2011).

[36] D. Proment and M. Onorato, Eur. J. Mech. B Fluids **34**, 1 (2012).

[37] K. Sakkaravarthi and T. Kanna, Eur. Phys. J. Spec. Top. **222**, 641 (2013).

[38] H. N. Chan, E. Ding, D. J. Kedziora, R. H. J. Grimshaw, and K. W. Chow, e-print No. 14-04: http://www.lboro.ac.uk/microsites/maths/research/preprints.

[39] S. Chen, Phys. Lett. A **378**, 1095 (2014).

[40] A. E. Kaplan, Phys. Rev. Lett. **55**, 1291 (1985).

[41] R. H. Enns, S. S. Rangnekar, and A. E. Kaplan, Phys. Rev. A **36**, 1270 (1987).

[42] B. A. Malomed, I. M. Skinner, P. L. Chu, and G. D. Peng, Phys. Rev. E **53**, 4084 (1996).

[43] A. V. Buryak and Yu. S. Kivshar, Phys. Rev. Lett. **78**, 3286 (1997).

[44] N. Akhmediev, J. M. Soto-Crespo, and G. Town, Phys. Rev. E **63**, 056602 (2001).

[45] J. M. Soto-Crespo, N. Akhmediev, and Ph. Grelu, Phys. Rev. E **74**, 046612 (2006).

[46] P. Dubard, P. Gaillard, C. Klein, and V. B. Matveev, Eur. Phys. J. Spec. Top. **185**, 247 (2010).

[47] A. Ankiewicz, D. J. Kedziora, and N. Akhmediev, Phys. Lett. A **375**, 2782 (2011).

[48] J. S. He, H. R. Zhang, L. H. Wang, K. Porsezian, and A. S. Fokas, Phys. Rev. E **87**, 052914 (2013).